

Jasper: ANNS Quantized for Speed, Built for Change on GPU

Hunter McCoy
Northeastern University
Boston, United States
mccoy.hu@northeastern.edu

Zikun Wang
Northeastern University
Boston, United States
wang.zikun@northeastern.edu

Prashant Pandey
Northeastern University
Boston, United States
p.pandey@northeastern.edu

Abstract

Approximate nearest neighbor search (ANNS) is a core problem in several machine learning and information retrieval applications. GPUs offer a promising path to high-performance ANNS: they provide massive parallelism for distance computations, are readily available in modern data centers, and can co-locate with downstream applications to reduce data movement.

Despite these advantages, current GPU-accelerated ANNS systems face three key limitations. First, real-world applications operate on evolving datasets that require fast batch updates, yet most GPU indices must be rebuilt from scratch when new data arrives. Second, high-dimensional vectors strain memory bandwidth, but current GPU systems lack efficient quantization techniques that reduce data movement without introducing costly random memory accesses. Third, the data-dependent memory accesses inherent to greedy search make overlapping compute and memory difficult, leading to reduced performance.

We present Jasper, a GPU-native ANNS system that achieves both high query throughput and full updatability. Jasper builds on the Vamana graph index and overcomes existing bottlenecks via three contributions: (1) a batch-parallel construction algorithm adapted for CUDA that enables lock-free streaming insertions, (2) a GPU-efficient implementation of RaBitQ quantization that reduces memory footprint up to 8 \times without the random access penalties, and (3) an optimized greedy search kernel that increases compute utilization, resulting in better latency hiding and higher throughput.

Our evaluation across five datasets shows that Jasper achieves up to 1.93 \times higher query throughput than CAGRA, the current state-of-the-art GPU index, and achieves up to 80% peak utilization as measured by the roofline model. Jasper’s construction scales efficiently to large datasets and constructs indices an average of 2.4 \times faster than CAGRA while providing updatability that CAGRA lacks. Compared to BANG, the previous fastest GPU Vamana implementation, Jasper delivers 19 – 131 \times faster queries.

ACM Reference Format:

Hunter McCoy, Zikun Wang, and Prashant Pandey. 2026. Jasper: ANNS Quantized for Speed, Built for Change on GPU. In . ACM, New York, NY, USA, 17 pages. <https://doi.org/10.1145/nnnnnnnn.nnnnnnnn>

Permission to make digital or hard copies of all or part of this work for personal or classroom use is granted without fee provided that copies are not made or distributed for profit or commercial advantage and that copies bear this notice and the full citation on the first page. Copyrights for components of this work owned by others than the author(s) must be honored. Abstracting with credit is permitted. To copy otherwise, or republish, to post on servers or to redistribute to lists, requires prior specific permission and/or a fee. Request permissions from permissions@acm.org.

Conference’17, Washington, DC, USA

© 2026 Copyright held by the owner/author(s). Publication rights licensed to ACM. ACM ISBN 978-x-xxxx-xxxx-x/YY/MM
<https://doi.org/10.1145/nnnnnnnn.nnnnnnnn>

1 Introduction

Nearest neighbor search is a fundamental problem in machine learning and information retrieval. The problem involves finding the k closest points to a query in a high-dimensional space. In this paradigm, complex data such as images, documents, or user profiles are embedded as vectors in a *metric space* (such as Euclidean, Manhattan, Hamming) that enables similarity to be measured through geometric distance. Applications span recommendation systems [31, 34], image retrieval [4, 30], anomaly detection [13, 27, 32], and increasingly, retrieval-augmented generation (RAG) for large language models [29, 41, 42], where relevant context must be retrieved from massive corpora in real time.

Traditional indexing structures such as $k-d$ trees [5] and quad trees [10] provide efficient exact nearest neighbor search in low dimensions, but scale poorly as dimensionality increases. The *curse of dimensionality* [24] causes distances between points to concentrate, with the ratio between nearest and farthest neighbors approaching one. This phenomenon undermines the spatial pruning heuristics that traditional indices rely upon, causing query complexity to degrade toward exhaustive linear scans. Modern embedding models routinely produce vectors with hundreds to thousands of dimensions, limiting the practicality of exact methods.

Approximate nearest neighbor search (ANNS) addresses this challenge by relaxing the exactness constraint. Rather than returning exact nearest neighbors, ANNS returns results within some acceptable error bound. This trade-off enables scalability to high-dimensional datasets. The three dominant paradigms for ANNS are: inverted file indices (IVF) [3, 20, 36, 44], locality-sensitive hashing (LSH) [7, 16, 25], and graph-based indices [8, 9, 12, 18, 21–23, 28].

Graph-based indices achieve the best recall-throughput trade-offs among these paradigms. Recent empirical studies have consistently demonstrated this advantage [18]. Graph-based indices construct a *navigable search graph* [21] where vertices correspond to vectors and edges encode neighborhood relationships. Nearest neighbor queries proceed via greedy traversal also known as *beam search*: starting from a designated entry point, the search iteratively expands the closest unvisited vertex until convergence, maintaining a frontier of the best (top k) candidates encountered.

Modern applications require updatable ANNS indexes. Real-world ANNS applications operate at massive scale and require continuous updates due to evolving datasets. Web-scale retrieval systems index billions of vectors: Facebook’s similarity search infrastructure handles over 200 billion embeddings [9], while Microsoft’s Bing uses DiskANN to search over a billion document vectors [2]. These systems must support both millions of queries per second and continuously index updates as new content arrives [34]. Music streaming, product recommendation, and RAG systems depend on scalable and updatable similarity search [35].

The case for GPU acceleration. GPUs offer massive parallelism that promises to accelerate ANNS to achieve high throughput and low latency. Graph-based ANNS is well-suited to leverage this parallelism because its core operations (pair-wise distance computations) are independent and can execute concurrently. Both index construction and search are dominated by distance computations, which can be performed in parallel across candidates. As dataset size and vector dimensionality grow, so does the available parallel work that GPUs can exploit.

Furthermore, GPUs are already widely deployed in settings where ANNS is most needed. Modern machine learning infrastructure runs on GPU clusters. Using GPUs for ANNS allows organizations to leverage existing hardware rather than provisioning separate CPU-based retrieval infrastructure. This co-location also reduces data movement: embeddings generated on GPU can be indexed and queried without costly transfers to CPU memory.

Challenges in exploiting GPU parallelism for ANNS. Modern GPUs offer thousands of execution units and memory bandwidth exceeding 2 TB/s [26], yet achieving peak performance for ANNS indexing and queries remains difficult. We identify three key challenges in exploiting the massive GPU parallelism.

1) *ANNS workloads need updatability.* Most current GPU indices require a rebuild from scratch in order to process new updates. This is due to limitations in how GPUs allocate and free memory. Real-world workloads such as anomaly detection [13] and RAG [29, 41, 42] require the ability to modify the index to incorporate new information.

2) *Greedy graph traversal creates irregular memory access patterns.* Unlike dense matrix operations where access patterns are known ahead of time, graph search follows data-dependent paths that vary per query. When different threads in a warp access non-contiguous memory locations, the GPU must issue multiple memory transactions, wasting memory bandwidth. This problem is made worse by the pointer-chasing nature of graph traversal, where each hop depends on the previous result.

3) *ANNS workloads are memory-bound rather than compute-bound.* Each vector dimension is read once, used for a single multiply-add in the distance computation, then discarded. With no data reuse, performance is limited by how fast data can be fetched from memory rather than how fast arithmetic can be performed. For a 128-dimensional float32 vector, the GPU performs 256 floating-point operations but must load 512 bytes of data, a ratio far below what modern GPUs can sustain at peak compute utilization. In our analysis in Section 6.5, we find that the state-of-the-art ANNS search kernels are very close to the peak memory capacity: to further improve performance, data transfer must be reduced.

Limitations of existing GPU ANNS systems. Existing GPU ANNS systems either lack updatability or suffer from poor performance. CAGRA [28], the current state-of-the-art GPU ANNS system, achieves high query throughput by employing a carefully optimized graph structure derived from NN-Descent. However, CAGRA’s graph construction algorithm is batch-oriented, and the system is not designed for incremental updates. In production settings where data arrives continuously, the inability to update the index without full reconstruction is a critical limitation.

BANG [39] is based on an updatable graph structure but suffers from severe performance penalties as it employs product quantization (PQ) [20]¹ for compressing the vectors. BANG extends the ANNS over Vamana [18] graph to GPUs and uses the underlying graph structure that enables updates (although BANG currently does not implement index updates). However, its reliance on PQ hurts performance. In Section 5, we discuss in detail the limitations of product quantization on GPUs.

Other GPU ANNS systems face their own constraints. GANNS [37] implements HNSW but struggles with the algorithm’s sequential construction dependencies. SONG [46] and GTS [47] target different index structures (fixed-rank graphs and trees, respectively) with different trade-off profiles. None of these systems simultaneously achieve state-of-the-art query performance, efficient construction, and support for streaming updates.

This paper. We present Jasper, a GPU-native ANNS system that addresses these challenges to achieve high query throughput while supporting dynamic index updates. Jasper makes three major contributions. First, we devise a new lock-free batch-parallel construction algorithm optimized for block-level parallelism in GPUs based on ParlayANN [23]. This enables lock-free streaming insertions with best-in-class construction performance, making Jasper the first high-performance GPU ANNS system to support incremental updates. Second, to overcome the irregular access patterns of graph traversal, we perform a systematic analysis of greedy beam search on GPUs and find that high occupancy and small beam widths are the crucial components for achieving high performance in beam search. We present a tuned beam search kernel that removes all extraneous components and achieve up to 1.93 faster query performance than CAGRA, the state-of-the-art GPU ANNS index. Third, we present the first GPU implementation of RaBitQ quantization [11]. Through systematic analysis, we show that existing GPU quantization methods like product quantization fail to deliver speedups due to scattered memory accesses. RaBitQ avoids these pitfalls and increases arithmetic intensity, shifting ANNS away from the memory-bound regime and enabling higher throughput on very high-dimensional datasets.

Contributions. We make the following contributions:

- **GPU-efficient quantization.** We present the first GPU implementation of RaBitQ [11], a quantization scheme that compresses vectors through randomized rotation and scalar quantization. Unlike product quantization, RaBitQ distance computation requires sequential memory access and simple arithmetic—no codebook lookups. This enables up to 8× memory reduction for 32-bit vectors while actually *improving* throughput for very high-dimensional datasets, as reduced memory traffic outweighs the modest computational overhead.
- **Optimized search kernel** We analyze the greedy search kernel and identify that for smaller vectors compute occupancy and block size dominate performance. Peak performance is reached at a block size of 32 and 100% occupancy due to better latency hiding between blocks in an GPU streaming multiprocessor (SM) (defined in Section 2.2). To achieve this, we devise a new search kernel that strips all unnecessary components to maximize the number of queries launched per SM. The performance of this kernel is

¹PQ is a quantization technique that reduces vector size by decomposing the original vector into a Cartesian product of independently quantized low-dimensional subspaces.

validated through both empirical benchmarking and roofline analysis [43]. The kernel achieves between 70%-80% of peak possible performance for its arithmetic intensity and achieves up to 50% higher FLOPS/s compared to CAGRA for the same query accuracy.

- **Optimized memory access patterns.** We introduce a tile-based loading scheme that issues blocked 16-byte loads across the threads in a warp simultaneously. Naive implementations either serialize loads through a single thread or issue element-wise loads across the warp (defined in Section 2.2). Our approach achieves both low latency and high throughput by partitioning vectors into 16-byte chunks processed in parallel.
- **Batch-parallel GPU construction.** We devise a new batch-parallel construction algorithm for GPU execution based on ParlayANN. Rather than using fine-grained locks that create serialization bottlenecks at high-degree vertices, our approach performs beam searches independently, accumulates candidate edges, sorts them by target vertex, and applies pruning in parallel without needing synchronization.
- **Systematic performance analysis.** We conduct a detailed empirical study of GPU ANNS optimization strategies. We characterize the trade-offs between per-query parallelism and memory-level parallelism, finding that optimal block sizes differ significantly across datasets. We perform roofline analysis [43] on the state-of-the-art search kernels and find that modern ANNS kernels are memory bound and execute at close to optimal throughput.

Results. Our evaluation on five standard ANNS benchmarks demonstrates:

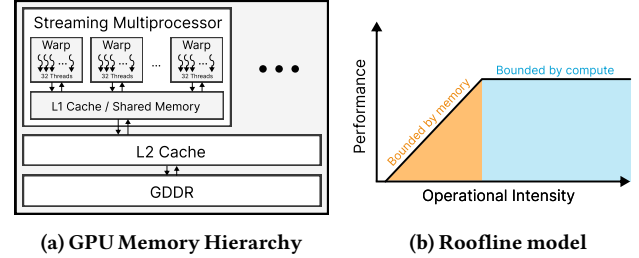
- Jasper achieves up to $1.93 \times$ higher query throughput than CAGRA, the state-of-the-art GPU index, while providing updatability that CAGRA lacks.
- Compared to BANG, the previous state-of-the-art GPU Vamana implementation, Jasper delivers $19 - 131 \times$ higher throughput.
- Jasper achieves peak throughput exceeding 13.1 million queries/sec on the BigANN dataset and over 3 million queries/sec on 1,536-dimensional OpenAI embeddings with RaBitQ quantization.
- Jasper’s has the fastest incremental and batch GPU construction: Jasper has a peak insertion throughput of 674K insertions per second and is $2.4 \times$ faster on average than CAGRA for index construction across five datasets.
- Our coalesced vector loading scheme improves memory access performance by up to 14% at low beam widths, with no throughput penalty at high beam widths.

2 Preliminary

This section describes the GPU execution and memory models relevant to building high-throughput ANNS indexes. We first explain the GPU execution model and how work is scheduled on the GPU. We then explain the GPU memory hierarchy and how it affects achieving peak performance. We then examine how these hardware characteristics affect existing GPU ANNS systems and introduce the roofline model [43] as a framework for analyzing their performance.

2.1 GPU execution model

A diagram of the GPU architecture is shown in Figure 1a. A GPU consists of multiple **streaming multiprocessors (SMs)**, each capable of hosting up to 1024 concurrent threads. Tasks on a GPU



(a) GPU Memory Hierarchy

(b) Roofline model

Figure 1: GPU memory hierarchy and roofline model.

are executed in a chunk of work called a **kernel**. Each kernel is a single-instruction, multiple-thread (SIMT) function that is executed in parallel by every thread. GPU kernels are executed as collections of *thread blocks* on SMs, each containing up to 1024 threads. Within a block, threads are subdivided into *warps* (groups of 32 threads) that share execution resources and issue memory operations cooperatively. As a result, performance is maximized when threads within a warp follow identical control flow and access contiguous or nearby memory locations. Warps can be further subdivided into *tiles* that divides the resources within a warp for multiple jobs.

ANNS workloads expose fine-grained parallelism during nearest neighbor search as pairwise distances can be computed independently in parallel. Each vector is examined by a *tile*, allowing multiple candidate vectors to be accessed and evaluated in parallel. Tiles are densely packed into warps: larger tiles increase per-probe parallelism by examining more individual vectors faster, while smaller tiles improve latency hiding by enabling additional concurrent memory requests within a warp.

The optimal block and tile configuration depends on the characteristics of the ANNS index, including memory layout, probe fan-out, and candidate filtering costs.

2.2 GPU memory model

The design of concurrent GPU data structures is fundamentally constrained by the underlying memory consistency model, which governs how memory operations from different threads become visible to one another. In contrast to CPUs that are sequentially consistent, modern GPUs implement a weak memory model based on Relaxed Memory Ordering (RMO) [1]. Under RMO, reads and writes may be freely reordered unless explicitly constrained, and a read in one thread that logically follows a write in program order from a different thread is not guaranteed to observe that write without additional synchronization. GPUs prioritize throughput over latency. With thousands of concurrent threads on GPUs, enforcing strong ordering requires expensive coherence traffic.

All threads within an SM share an L1 cache, which is not coherent with L1 caches on other SMs. These per-SM caches connect to a globally coherent L2 cache, which in turn backs the GPU’s main memory (GDDR).

This shared L1 cache is crucial for achieving high performance in GPU applications. A section of this cache can be designated as **shared memory**. Unlike a regular cache, this shared memory is directly addressable and acts as both a scratchpad and a means of efficiently passing data between threads in a block. The amount of

shared memory utilized affects the potential **occupancy**, the maximum number of blocks that can be scheduled simultaneously in an SM. Every block in a kernel will request the same amount of shared memory. If the total amount of shared memory is more than the SM can support, the occupancy will be reduced, leading to fewer blocks running in parallel and some threads sitting idle.

To achieve high performance on GPUs, we must design GPU kernels for ANNS index construction and querying that efficiently utilize shared memory to maximize occupancy. Specifically, we aim to keep all frequently used data in shared memory and carefully select data structures that fit within the available resources without reducing maximum occupancy.

2.3 Roofline model

The roofline model [43] is a simple, quantitative performance model that bounds the attainable performance of an application on a given architecture using two hardware limits: peak compute throughput and peak memory bandwidth. Performance is expressed as a function of *arithmetic intensity*, defined as the ratio of useful operations to bytes transferred from main memory. For low arithmetic intensity kernels, performance is limited by memory bandwidth and grows linearly with arithmetic intensity; for high intensity kernels, performance saturates at the hardware's peak compute rate. Graphically, these bounds form a "roofline" (see Figure 1b): a sloped bandwidth roof intersecting a flat compute roof, making it easy to see whether a workload is memory-bound or compute-bound and how close it is to hardware limits.

The roofline model is widely used to guide performance optimization and architectural analysis as it abstracts complex microarchitectural details into a small set of measurable parameters. Optimizations that increase data reuse (e.g., blocking, caching, fusion) move kernels rightward by increasing arithmetic intensity, while vectorization, parallelism, and instruction-level efficiency move kernels upward towards the compute roof. Extensions of the model incorporate multiple memory levels, ceilings for specific bottlenecks, and heterogeneous devices, but the core insight remains: achievable performance is fundamentally constrained by the balance between computation and data movement. This framing has proven effective for reasoning about performance portability across CPUs, GPUs, and accelerators, and for communicating optimization priorities in both systems and data-intensive workloads. *We use the roofline model to evaluate both the achieved and potential performance of ANNS indices on GPUs.*

3 Vamana Index

In this section, we cover the Vamana algorithm graph structure, construction and query algorithm, and the batch-parallel construction algorithm. Our system Jasper employs the Vamana graph [18], a directed proximity graph designed to support efficient greedy search with bounded out-degree, to build the approximate nearest neighbor search (ANNS) index. We choose the Vamana graph as it supports both a fast and accurate greedy search and an efficient parallel construction algorithm introduced in ParlayANN [23]. We describe how we develop GPU-accelerated Vamana index along with several GPU optimizations in the next section.

3.1 Graph definition

The Vamana index is a directed graph $G = (V, E)$ constructed over a set of data vectors $V = \{x_1, \dots, x_N\}$, where N is the total number of vectors. Each node maintains an adjacency list of at most R outgoing edges. A distinguished entry point $s \in V$ is used to initialize both graph construction and query traversal.

The edge set E is selected to ensure that the graph remains sparse while preserving navigability. For a given vertex in the graph and query vector, there is a high probability that one of the outgoing edges of the vertex leads to a vertex that is closer to the query. This property means that greedy search will converge to a set of points close to a target query and is critical for enabling low-latency approximate search.

3.2 Vamana construction algorithm

The original Vamana construction algorithm starts with all vertices contained within a graph with a random set of edges with maximum outgoing degree R . Vamana graph construction proceeds incrementally to refine the graph one vertex at a time. Refinement of vertices proceeds in two phases. First, Vamana uses **BEAMSEARCH** to identify candidate neighbors in the existing graph for the new vertex. Second, Vamana applies a pruning procedure, **ROBUSTPRUNE**, to reattach the vertex to the graph while enforcing a strict bound on the out-degree.

Algorithm 1: BeamSearch (DiskANN)

```

Input: Graph  $G$ ,  

       query vector  $q$ , beam width  $K$ , start vertex  $m$  (medoid)  

Output: Frontier  $F$  of  $K$  nearest neighbors, visited set  $V$   

 $F \leftarrow \{m\}$  (priority queue by distance)  

 $V \leftarrow \emptyset$   

while there exists an unvisited vertex  $u \in F$  do  

  Mark  $u$  visited:  $V \leftarrow V \cup \{u\}$   

  for each neighbor  $v$  of  $u$  do  

    if  $v \notin V$  then  

      Compute distance  $d(q, v)$   

      Insert  $v$  into  $F$  with priority  $d(q, v)$   

    if  $|F| > K$  then  

      Remove furthest elements from  $F$  until  $|F| = K$   

return  $(F, V)$ 

```

Beam search. Given a vector x to be inserted, the construction algorithm performs an approximate nearest neighbor search in the current graph using **BEAMSEARCH**. The pseudocode for this procedure is shown in Algorithm 1. The search is initialized at a designated start vertex, typically chosen as the *medoid* (the vector closest to the center) of the dataset.

BEAMSEARCH maintains two sets: (i) a *frontier*, which stores the K closest candidate vertices discovered so far, ordered by increasing distance to the query vector x , and (ii) a *visited list*, which records all vertices whose outgoing edges have been explored. At each iteration, the algorithm selects the closest vertex in the frontier that has not yet been visited, loads its outgoing edges, computes the distance between x and each neighbor, and inserts newly encountered vertices into the frontier.

If the size of the frontier exceeds the beam width K , the furthest candidates are discarded. This expansion process continues until all vertices in the frontier have been visited. The procedure returns both the final frontier, representing approximate nearest neighbors of x , and the full visited list, which captures the local search region explored during insertion.

Edge attachment. Once `BEAMSEARCH` completes, the new vertex x is attached to the graph using the vertices in the visited list. Initially, bidirectional edges are added between x and each vertex in the visited list, temporarily allowing the out-degree of affected vertices to exceed the maximum degree bound R .

Algorithm 2: RobustPrune (DiskANN)

Input: Node p , candidate neighbors $N(p)$, degree cap R , pruning factor α , distance d
Output: Pruned neighbor set $N'(p)$
Sort $N(p)$ by $d(p, \cdot)$ (closest first)
 $N'(p) \leftarrow \emptyset$ (initialize as empty);
while $|N'(p)| < R$ and $N(p)$ not empty **do**
 $p^* \leftarrow$ extract closest from $N(p)$
 Add p^* to $N'(p)$
 for each $p' \in N(p)$ **do**
 if $\alpha \cdot d(p^*, p') \leq d(p, p')$ **then**
 Discard p' from $N(p)$
 else
 Keep p' in $N(p)$
return $N'(p)$

Robust prune. To restore the degree bound, Vamana applies the `ROBUSTPRUNE` procedure to any vertex whose outgoing edge list exceeds R (maximum out degree). The pseudocode for this procedure is shown in Algorithm 2. Given a vertex p , `ROBUSTPRUNE` takes the current set of outgoing neighbors and sorts them by increasing distance from p . The algorithm iteratively selects the closest remaining neighbor p^* and adds it to the pruned adjacency list. For each remaining candidate neighbor p' , `ROBUSTPRUNE` compares the distance $d(p^*, p')$ to the distance $d(p, p')$. If

$$d(p^*, p') \leq \alpha \cdot d(p, p'),$$

then p' is removed from consideration. This process repeats until either the pruned adjacency list reaches size R or no candidates remain.

Intuitively, `ROBUSTPRUNE` removes edges that are redundant due to the existence of a strong two-hop path: a direct edge from p to p' is discarded if p' can be reached via a significantly closer neighbor p^* . The parameter $\alpha > 1$ controls the aggressiveness of pruning and trades off graph sparsity for navigability.

Together, `BEAMSEARCH` and `ROBUSTPRUNE` allow Vamana to incrementally construct a bounded-degree proximity graph that preserves long-range connectivity while supporting efficient greedy traversal during query time.

3.3 ParlayANN

ParlayANN [23] is an extension of the Vamana construction algorithm that addresses a fundamental scalability bottleneck in parallel

graph construction by adopting a batch-parallel insertion scheme. While the original DiskANN [18] algorithm supports inserting points in parallel, it relies on fine-grained locks to update adjacency lists. In practice, this design leads to significant contention on high-centrality vertices, such as the *medoid*. During the greedy search, high-centrality vertices are frequently traversed, and concurrent insertions attempt to add edges to these vertices simultaneously, resulting in serialization that limits parallel scalability.

ParlayANN eliminates this bottleneck by replacing lock-based updates with a lock-free, batch-parallel construction strategy. The core idea is to decouple graph traversal from graph mutation, allowing expensive updates to be applied in parallel without contention.

Algorithm 3: Batch Insertion (ParlayANN)

Input: Batch of new points B , current graph G , beam width K , degree cap R
Output: Graph G updated with B
Step 1: Local candidate generation
for each $x \in B$ **do in parallel**
 $(F, V) \leftarrow$ BeamSearch($G, x, K, G.medoid$)
 $E_x \leftarrow \{(x, v) : v \in V\}$ // add edges for new nodes
Step 2: Global edge collection
 $E \leftarrow \bigcup_{x \in B} E_x$ // concatenate edge lists
Step 3: Semisort and parallel pruning
Group E by endpoint using **Semisort**
for each vertex u touched by E **do in parallel**
 $N'(u) \leftarrow$ RobustPrune($u, N(u) \cup E[u], R$)
 Update adjacency list of u with $N'(u)$
return G

ParlayANN restructures graph construction into two distinct, parallelizable phases, as shown in Algorithm 3. In the first phase, `BEAMSEARCH` (Algorithm 1) is executed independently and in parallel for each vertex to be inserted. Each search operates on a read-only snapshot of the current graph and produces a set of candidate edges corresponding to the vertices encountered during traversal. Importantly, no adjacency lists are modified during this phase.

Instead of applying updates immediately, all candidate edges produced by the batch are written to a temporary edge collection. This collection is then *semisorted*, grouping edges by their target vertex at substantially lower cost than a full sort. Semisort guarantees that all candidate edges incident to a given vertex are co-located, enabling subsequent processing to be performed independently per vertex.

In the second phase, `ROBUSTPRUNE` (Algorithm 2) is applied in a batch-parallel design. Each vertex that has received new candidate edges is assigned a unique thread, which merges the proposed edges with the existing adjacency list and applies `ROBUSTPRUNE` to enforce the maximum out-degree constraint R . Because all edges incident to a vertex are processed by a single thread, this phase requires no locks or cross-thread synchronization.

This lock-free design removes contention around centrally located vertices and allows ParlayANN to efficiently exploit multicore

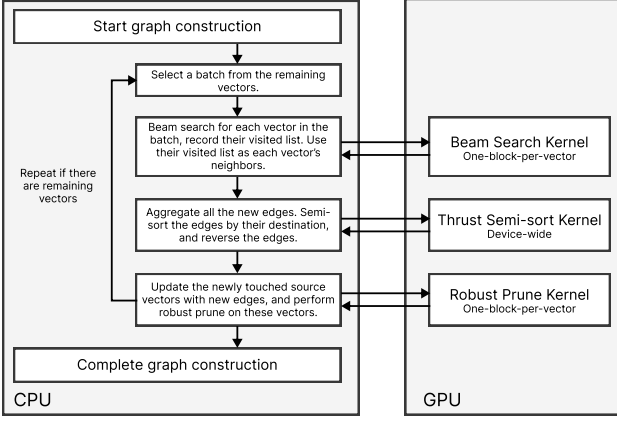


Figure 2: Batch graph construction pipeline in Jasper.

parallelism. The key insight is that the pruning step, which determines the final neighborhood structure and dominates construction cost, can be fully decoupled from concurrent graph traversals by deferring updates and processing them in parallel batches. As a result, ParlayANN achieves significantly faster index construction while preserving the structural guarantees of the Vamana graph and maintaining comparable query performance and accuracy.

3.4 Why Vamana index is well suited for GPUs?

Compared to many alternative ANN indices, the Vamana graph offers a high degree of parallelism across both index construction and query execution, enabling efficient use of modern GPUs. Its construction is inherently parallel: vertices are processed independently, each following a predictable sequence of steps that minimizes thread divergence. Distance computations and graph traversal both expose fine-grained parallelism. Vamana also supports efficient incremental updates. Each insertion performs a bounded beam search over a small subset of vertices and adds at most $2R$ edges, keeping overhead predictable. By comparison, update procedures for methods such as NN-Descent can be substantially more expensive, as multiple refinement rounds are required and any visited node may become a neighbor. Prior work shows that Vamana matches or exceeds alternative graph indices in search quality across diverse datasets, making it a strong foundation for high-performance, updatable ANNS [18].

4 Jasper: A GPU native ANNS system

This section presents the design of Jasper. The central challenge in GPU-based ANNS is achieving high utilization on an irregular, data-dependent, memory-intensive workload. Prior systems sacrifice either compute efficiency or memory bandwidth; Jasper achieves both simultaneously. We introduce a re-architected greedy beam search that restructures both the algorithm and its data structures around GPU execution constraints, exposing sufficient parallelism to saturate compute units while maintaining coalesced memory access patterns that approach peak bandwidth. We also redesign the batch-parallel construction algorithm for GPU execution, enabling lock-free streaming insertions. We evaluate how construction throughput scales with batch size and index size, demonstrating that

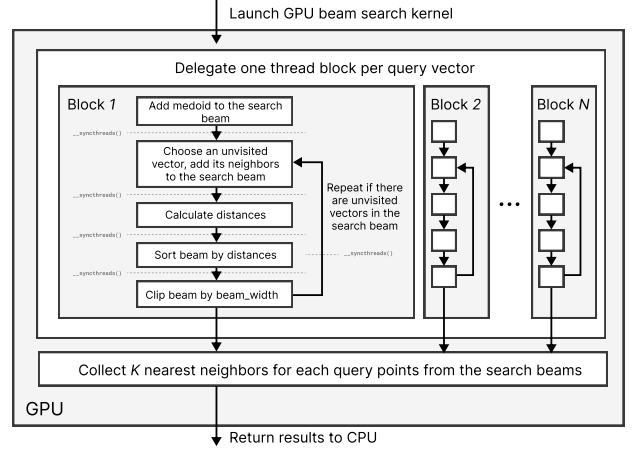


Figure 3: ANNS query pipeline in Jasper.

Jasper maintains high insertion rates even as the index grows by an order of magnitude.

4.1 Block-per-query execution model

A central design decision in Jasper is to assign a full CUDA thread block to each query or inserted vector. This block-per-query execution model allows us to precisely control how parallelism is applied at each stage of the beam search and to tailor execution to the GPU's architectural constraints. Compute-intensive phases, such as distance computations, are parallelized across all threads in a large block, while more irregular phases, such as candidate expansion and graph traversal, are partially serialized to limit control-flow divergence. This hybrid structure enables high utilization while accommodating the irregular access patterns inherent to graph-based ANN search.

When each query is executed in a single thread block, we can store the related information (e.g., beam frontier, candidate buffers, intermediate distances) in the shared memory. This significantly reduces global memory traffic and allows frequent reuse of data across threads. However, the choice of block size (i.e., number of threads in a CUDA block) introduces a fundamental trade-off between per-query compute throughput and memory-level parallelism (MLP). Larger blocks allocate more threads to a single query, increasing arithmetic throughput, instruction-level parallelism, and register reuse. Conversely, smaller blocks allow more queries to execute concurrently, increasing the number of outstanding memory requests and improving the GPU's ability to hide global-memory latency.

The relative importance of this trade-off depends strongly on on dataset characteristics. For low-dimensional vectors, where distance computation is inexpensive relative to memory latency, the benefits of increased MLP dominate. In this memory-bound regime, reducing the block size allows more concurrent queries per streaming multiprocessor (SM), increasing effective throughput even though each query receives fewer compute resources. For example, on BigANN, where vectors are only 128 bytes, we find that smaller block sizes are strictly beneficial up to the maximum occupancy of 32 blocks per SM.

For high-dimensional datasets such as Gist, distance computation becomes the dominant bottleneck. Our measurements show

that dot-product evaluation in Gist consumes 17.6 \times more cycles than memory operations. In this compute-bound regime, reducing block size directly degrades performance by limiting per-query parallelism, reducing register reuse, and lowering arithmetic throughput. Increased MLP provides little benefit when computation dominates, and smaller blocks therefore reduce overall throughput. As a result, the optimal block size is dataset dependent and closely tied to the compute–memory balance of the distance kernel: *memory-bound workloads benefit from higher concurrency and MLP, while compute-bound workloads require maximal per-query compute resources.*

Optimizing distance calculations. We observe that the square root operation accounts for over 40% of Euclidean distance computation time. Since square root is monotonic over positive reals, we safely elide it and compare squared distances instead, preserving correctness while significantly reducing compute overhead.

Optimizing beam search through kernel fusion. We further optimize the beam search process by fusing multiple phases into one single kernel, merging distance computation, frontier sorting, and neighbor expansion into one kernel executed by one block. By merging these three phases together, we avoid the cost of repeated kernel launch, and we can accelerate memory accesses by keeping all the information in shared memory. Kernel fusion is a common GPU optimization technique that is also used by CAGRA [28].

4.2 Optimizing BEAMSEARCH for GPUs

Our GPU version of BEAMSEARCH diverges from ParlayANN’s BEAMSEARCH due to the difference between CPU and GPU parallelism. We are limited by the computing model and amount of resources when running BEAMSEARCH on GPU. This section discusses the trade-offs we employ for GPUs. The BEAMSEARCH algorithm in ParlayANN is serial for each query, as there is limited parallelism in CPU to assign one thread to each query. On the GPU, we have an order of magnitude more threads. To fully saturate the GPU and achieve high performance, we must parallelize the internal components of BEAMSEARCH.

Different hash table choices. A major source of divergence arises from ParlayANN’s use of a lossy hash table during beam search. The original algorithm employs a fixed-size (512-slot) hash table with direct replacement to track previously visited vertices and prune duplicates. On CPUs, this structure is accessed sequentially within a single thread, yielding deterministic behavior. On GPUs, preserving this access pattern would require serializing hash table operations across cooperating threads, severely limiting throughput. Parallelizing these operations improves performance but introduces non-determinism. Additionally, we find that this hash table does not significantly affect accuracy or search throughput on the GPU. Removing the hash table further reduces shared memory pressure and allows Jasper to schedule more queries per block.

Different merge order. Jasper employs a different candidate merge order during beam search. ParlayANN implements a deferred-merge optimization, which postpones sorting and merging when candidate lists are smaller than a fixed fraction of the beam width. With non-deterministic hash tables on GPU, we cannot guarantee this mechanism produces the same candidate list order each time. Empirically, we find that removing the lossy hash table and deferred merging materially affects index quality or query accuracy. Consequently,

Jasper removes both features, simplifying control flow, preserving determinism, and eliminating a major source of divergence.

Limited shared memory on GPU. Finally, divergence is further amplified by shared memory constraints. Cooperative execution requires per-query shared data structures, which limits occupancy and reduces the GPU’s ability to hide memory latency. We deliberately accept this trade-off: tighter shared-memory budgets and higher intra-warp divergence enable greater locality and reuse, which are critical for irregular ANNS workloads. As shown in our roofline analysis in Section 6.5, this design remains competitive and when combined with query reordering in Jasper RaBitQ, can significantly increase operational intensity.

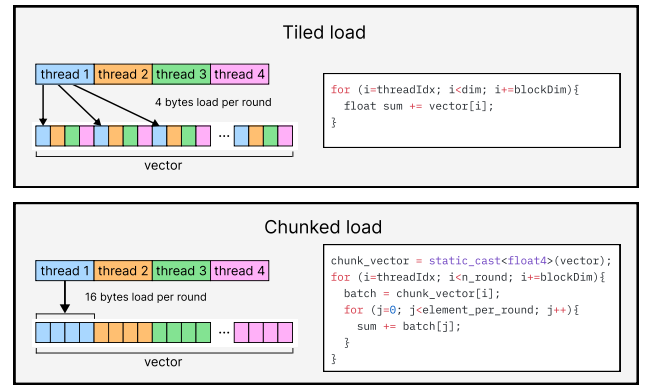


Figure 4: Comparison of the two different load strategies tested in Jasper: tiled loads load one object per thread in the tile at a time, whereas the chunked load strategy loads a fixed amount of data (16 bytes) per thread and has each thread work on all objects loaded in that chunk.

Vector load optimization. To maximize performance, we optimize how vector data is loaded. By default, when a warp accesses a large object, the compiler emits a sequence of 16-byte loads issued by a single thread, which limits latency hiding. Conversely, element-wise loads distribute requests across threads but reduce effective bandwidth.

We address this by partitioning each vector into 16-byte chunks and assigning one chunk to each thread. Threads load query and candidate chunks in parallel, compute partial distances locally, and repeat until the entire vector is processed. A block-wide reduction then produces the final distance. This scheme issues multiple coalesced 16-byte loads simultaneously, achieving near-peak bandwidth.

As shown in Figure 4, this optimization improves latency-sensitive regimes. For small beam widths, where search is latency-bound, we observe a 14% speedup. For large beam widths, where throughput dominates, optimized loads match baseline throughput without loss. These benefits apply equally to floating-point vectors and RaBitQ-quantized vectors. Combined with RaBitQ’s (a vector quantization scheme we discuss in Section 5) up to 50% reduction in data movement, optimized loading yields substantial end-to-end gains in beam search performance.

Dataset	Index Size	Construct Budget	Batch Size
BigANN 100M	38.5GB	41.5GB	1M
Deep 100M	64.1GB	15.9GB	400K

Table 1: Batch size to achieve maximum throughput during updates in Jasper.

4.3 Batch construction on GPUs

To support high-performance ANNS index construction on GPUs, we adopt the bulk construction approach from ParlayANN [23]. ParlayANN leverages *fork-join parallelism* via ParlayLib [6] and performs a *semisort* to group edges before insertion, enabling lock-free parallel updates. Specifically, ParlayANN uses fork-join parallelism to divide larger tasks (e.g., semisorts) into smaller tasks and assigns multiple threads to execute them. However, GPUs do not support this level of dynamic parallelism, as each kernel can only be launched with a fixed number of threads. Moreover, we aim to minimize the number of kernel launches to avoid launch overhead. Therefore, we fused different construction steps into self-contained GPU kernels (see Figure 2). While this removes some scheduling flexibility, it allows us to retain the scalability benefits of batch-parallel searching and pruning while conforming to the GPU execution model.

GPU-efficient pruning. We implement a hybrid strategy for ROBUSTPRUNE. Outgoing edges generated by beam search are accumulated alongside existing edges requiring pruning and stored in a unified buffer. This buffer is fully sorted by vertex ID and distance using CUDA Thrust library. On the other hand, ParlayANN uses a semisort and then sorts the neighbors by distance with one thread inside of ROBUSTPRUNE. We identify that a full sort yields better load balance on GPUs as individual threads are relatively weak and uneven work distribution is costly. Each edge list is then pruned by assigning a full SM of 1024 threads as this phase is dominated by distance computations and benefits from high parallelism.

4.4 Scalability with batch size for updates

To fully utilize the memory capacity provided by modern GPU architectures during index construction, we choose different maximum construction batch sizes based on the dataset size and graph dimensionality. When Jasper constructs the graph index, both the vectors and the graph index are stored in the GPU’s device memory. This design allows the index to be built entirely on the GPU, avoiding the slow PCIe data transfers between host and device memory. Consequently, the remaining device memory serves as the available workspace for the construction algorithm.

Using the NVIDIA A100 GPU as an example, it provides 80 GB of on-device memory. For the BigANN 100M dataset, the combined size of the dataset and graph index is 38.5 GB, leaving 41.5 GB available for graph construction. For the Deep 100M dataset, the total size is 64.1 GB, leaving 15.9 GB of available memory. In our experiments, we found that the optimal batch size for index construction is 1,000,000 vectors per batch for BigANN and 400,000 vectors per batch for Deep, corresponding to the available memory budgets described in Table 1.

Variable Name	Description
m	Quantize bits per dimension
c	Centroid vector
v	Original data vector
q	Original query vector
o	Rotated and normalized $v - c$
\bar{o} or data	Quantized data vector
Δ_x	The rescaling factor of \bar{o} from o
data_add	$ v - c ^2 + 2 \cdot v - c ^2 \cdot \frac{\langle c, \bar{o} \rangle}{\langle o, \bar{o} \rangle}$
data_rescale	$-2 \cdot \Delta_x / \langle o, \bar{o} \rangle$
rotated_query_vector	Rotated and normalized $q - c$
query_add	$ q - c ^2$
query_sumq	$\sum (q - c) \cdot \frac{2^{m-1}-1}{2}$

Table 2: RaBitQ variable definitions.

5 Vector quantization

Modern embedding models produce vectors spanning hundreds to thousands of dimensions, with per-vector sizes ranging from 96 bytes to over 6000 bytes as shown in BigANN benchmarks [33]. Because ANNS is memory-bound—each vector element is read once, used for a single arithmetic operation, and discarded—reducing vector size directly improves query throughput.

To reduce per-vector storage and I/O costs while preserving search accuracy, we consider *quantization*, which compresses vectors while approximately preserving distances. The most widely used approach for ANNS is *product quantization* (PQ) [20]. PQ divides each vector into K disjoint subvectors and quantizes each independently using a small codebook of 256 centroids. Each subvector is then encoded as a single byte indicating its nearest centroid, compressing a high-dimensional vector to just K bytes. Distance computation uses a precomputed *lookup table* storing centroid-to-centroid distances for each subspace. This results in significant compression with modest accuracy loss, as error arises only from the approximation of each subvector by its nearest centroid.

Although PQ compresses vectors effectively, its *lookup table* access pattern results in lower throughput on GPUs. GPU memory is organized into 32-byte *sectors* that are loaded atomically—reading a single 4-byte distance entry wastes the remaining 28 bytes, causing 8× read amplification. A straightforward solution is to place the lookup table in shared memory, but even a modest configuration ($K = 32$) requires $32 \times 256 \times 256 \times 4$ bytes (8 MB), far exceeding shared memory capacity. We implemented PQ in Jasper but found that throughput was strictly worse than unquantized search for all configurations tested. Similar conclusions regarding the PQ performance on GPU has been presented in prior research [28].

5.1 RaBitQ quantization

To effectively use quantization on the GPU, we must avoid random memory accesses during distance computation. Previous GPU implementations treat quantization as a trade-off: smaller vectors and lower memory I/O at the cost of lower throughput [28, 39]. We show this trade-off is not fundamental. Jasper employs RaBitQ [11], a quantization method that is well suited for GPUs. RaBitQ requires

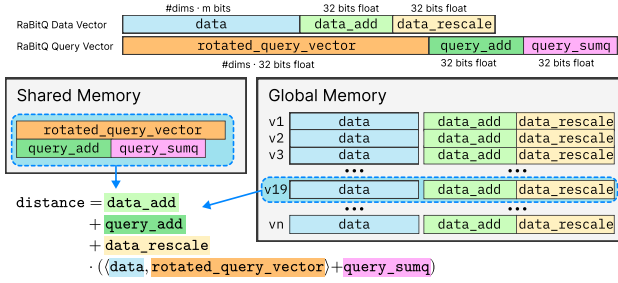


Figure 5: During distance calculation, RaBitQ loads query vector and its metadata from shared memory, and it loads quantized data vector and its metadata from global memory.

only sequential memory access, simple arithmetic, and requires no lookup tables.

RaBitQ estimates the distance using the inner product between the quantized data vector with the query vector. Table 2 shows how the related variables and quantized vector are calculated. RaBitQ compresses the data vectors by first normalizing them and applying a random rotation matrix. With high dimensional vectors, any rotated dimensions are likely tightly clustered around 0: according to the Johnson-Lindenstrauss lemma [19], the value of any coordinate is no further than $\frac{2}{\sqrt{D}}$ away from 0 with high probability. This allows RaBitQ to treat each dimension as an unbiased distribution and enables simple scalar quantization. RaBitQ encodes each dimension with m bits along with two floating point metadata: data_rescale and data_add. In total, the size of the quantized vector is

$$\#dims \cdot m \text{ bits} + 2 \cdot \text{sizeof}(\text{float})$$

During querying, RaBitQ applies the same rotation matrix to the query vector, and RaBitQ calculates each query vector's metadata: query_add and query_sumq. Figure 5 shows how RaBitQ estimates distances solely based on quantized vectors and rotated query vectors. The RaBitQ estimator reduces the L2 distance calculation to estimating the inner product between the quantized data vector (data) and rotated query vector (rotated_query_vector). This process estimates the vector distance without branching or randomized memory accesses while most of the values are pre-computed, which makes it highly suitable for GPU execution. RaBitQ's sequential memory access during distance calculation also allows us to utilize the same loading technique for exact vector loading in Section 6.6.

Jasper integrates GPU-accelerated RaBitQ. RaBitQ achieves 2 \times compression for 8-bit vectors and up to 8 \times for 32-bit vectors. On datasets with large dimensions, our results demonstrate that Jasper with RaBitQ performs significantly better than our exact distance calculation version. In Section 6.6, we perform a detailed analysis between RaBitQ's performance and PQ's performance.

6 Evaluation

In this section, we evaluate the performance of Jasper against four state-of-the-art ANNS indices: three GPU-based and one CPU-based index. We evaluate the construction, query, and update performance across five real-world datasets varying in size and number of dimensions. We further evaluate the effectiveness of Jasper in saturating

Name	Data Type	Dimensions	Distance Type	Size
BigANN	uint8	128	Euclidean	100M
Deep	float32	96	Euclidean	100M
Gist	float32	960	Euclidean	1M
OpenAI-ArXiv	float32	1536	Euclidean	2.3M
Yandex Text-to-Image	float32	200	Inner product	10M

Table 3: Details of datasets employed in our evaluation.

GPU resources using the roofline model [43]. Finally, we perform a series of micro-benchmarks to evaluate the impact of various GPU-specific optimizations introduced in Jasper and discuss how these are broadly applicable for optimizing other GPU-accelerated systems. Jasper source code and instructions to perform benchmarks are publicly-available at <https://github.com/saltsystemslab/JasperGPUANNS>.

6.1 Experimental setup

We evaluate all systems on along three dimensions:

- **Construction throughput:** measured as the total time required to build the index used in subsequent experiments.
- **Query throughput:** reported as the number of ANN queries completed per second.
- **Recall:** which measures the accuracy of the Top- K results and is defined as $\text{Recall}@K = \frac{\# \text{ of exact Top-}K \text{ results returned}}{K}$. We report recall at 1@1, 10@10, 50@50, and 100@100.

Hardware. All CPU experiments are conducted on an Intel(R) Xeon(R) CPU E5-2680 v4 with 14 physical cores (28 hardware threads) at 2.40 GHz. GPU experiments are run on an NVIDIA A100 (SM80) with 80 GB of HBM memory using CUDA 12.9.

Datasets. For evaluation, we select the following datasets taken from the Big_ANN_Benchmarks [33] repository, summarized in Table 3.

- BigANN: 100 million 128-dimensional uint8 vectors with Euclidean distance from the SIFT collection. There are 10K vectors in the test set.
- Deep/Yandex: 100 million PCA-reduced, normalized GoogLeNet embeddings (96-dimensional float32). Euclidean distance and 10K queries.
- Gist: 1 million 960-dimensional float32 vectors with euclidean distance and 1K query vectors in the test set.
- OpenAI-ArXiv: 2.3 million 1536-dimensional float32 embeddings of Arxiv papers. Query set is 10K vectors.
- Text2Image: 10 million 200-dimensional float32 image embeddings from the Se-ResNext-101 model. Distance is maximum inner product search (MIPS) and there are 10K queries in the test set.

ANNS indices. We compare Jasper to the following ANNS indices:

- **CAGRA** [28]: The state-of-the-art in GPU index construction. CAGRA constructs a graph index using NN-Descent [40]. NN-Descent iteratively improves graph connectivity by expanding each node's neighborhood through 2-hop neighbors. The resulting graph is well-connected but too dense for GPU memory. CAGRA addresses this with a three-phase pruning algorithm: edges are sorted by length, redundant edges with good 2-hop alternatives

Dataset	Jasper	CAGRA	ParlayANN	GANNS	Jasper Speedup over CAGRA
BigANN	679.8	1323.3	2797.5	-	1.95×
Deep	785.0	825.6	7818.3	-	1.05×
Gist	14.8	14.1	450.7	151.9	0.95×
OpenAI	120.1	127.8	4043.1	899.2	1.06×
Text2Image	88.7	619.2	433.6	1017.4	6.98×

Table 4: Index construction time in seconds for various ANNS indexes. ParlayANN is constructed on CPU. GANNS could not finish construction on BigANN and Deep 100M datasets.

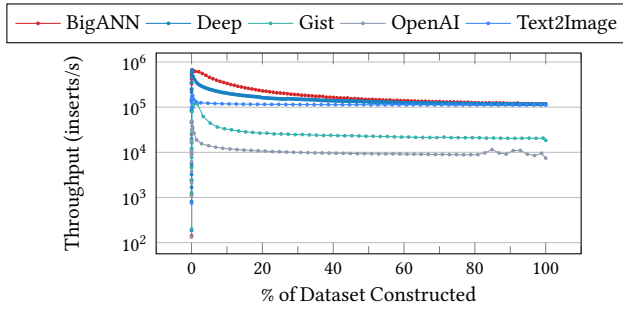


Figure 6: Jasper incremental construction throughput. Y-axis is on log-scale.

are removed, and finally the graph is merged with its reverse and pruned again to produce the final index.

- **BANG** [39]: BANG extends the query execution of DiskANN [18] to GPUs. BANG does not perform construction and requires a preconstructed Vamama graph from DiskANN. BANG uses product quantization to reduce the size of the vectors. The quantized vectors are stored in the GPU memory while the graph and full vector data are stored in DRAM. The entirety of a streaming multiprocessor (SM) is used for each query. One thread is used for each distance calculation, as distances can be calculated using only PQ table lookups. To process queries more efficiently, Bloom filters are used to represent the visited list, lowering the memory requirements for searching.
- **GANNS**: GANNS [45] is an implementation of the HNSW graph algorithm optimized for GPUs. To optimize for GPU execution, GANNS uses lazy data structures - rather than maintain a priority queue, GANNS maintains two lists (frontier and visited) and only occasionally updates the lists to mark vertices as visited. They avoid the use of a hash table for marking visited vertices during queries, and use multiple thread blocks per query. The construction algorithm for HNSW graphs is difficult to parallelize, so GANNS constructs many small graphs in parallel and then sequentially merges them. GANNS does not support dataset with 100 million vectors.
- **ParlayANN**: ParlayANN is the state of the art for Vamana construction and implements the batch-parallel construction algorithm. This algorithm is discussed in more detail in Section 3.3.

For all indices the graph size is held constant at $R=64$, so each vertex has at most 64 outgoing edges.

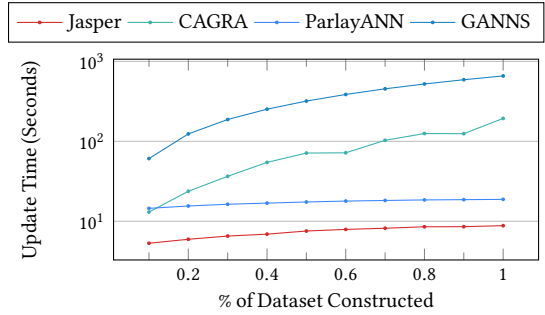


Figure 7: Incremental vs non-incremental construction throughput for BigANN 10M. Jasper and ParlayANN support batch incremental updates. CAGRA and GANNS do not support updates and need to be built from scratch at each step. Y-axis is on log-scale.

6.2 Index construction

Here we evaluate the index construction performance of Jasper against other ANNS indexes.

Bulk construction. In this benchmark, datasets are constructed in one shot. Results are shown in Table 4. We measure the overall construction throughput as the ratio of the number of vectors indexed and total construction time. Jasper achieves the highest construction throughput on all datasets except Gist, with peak throughput of 674K inserts/sec on BigANN. CAGRA is the fastest dataset for Gist construction with peak throughput of 70.6K inserts/sec. Jasper has comparable speed with CAGRA when constructing Gist. However, due to the smaller number of vectors in Gist (1 million), the construction batch size for Jasper is bounded to 2% of the total dataset, resulting in under-utilization of GPU parallelism. ParlayANN while running on CPU (28 threads) is between 4–30× slower than Jasper. GANNS is another GPU-based ANNS index but is between 7–11× slower than Jasper. Furthermore, GANNS does not support construction on 100M datasets as it is constrained due to `int32` datatype being employed to index into the vector array. 100M vectors with 128/96 dimensions require 64-bit datatype for indexing.

Incremental construction. Figure 6 shows how Jasper’s construction throughput changes as the index grows. We build the index incrementally, inserting vectors in batches of 2% of the total dataset. Across all datasets, throughput decreases as the index grows, but the slowdown is sub-linear in index size. For example, on Deep, Jasper inserts 251K vectors/sec when the index is at 5% capacity (500K vectors). When the index reaches 99% capacity (9.9 million vectors), throughput drops to 116K vectors/sec. This is less than a 2.2× slowdown despite a 20× increase in index size, demonstrating that Jasper maintains efficient insertion performance even as the index grows large.

Figure 7 illustrates why incremental construction matters. We measure the time required to add a 10% slice of new vectors to an already-constructed index, simulating a common production scenario where new data arrives after the initial index is built. Jasper and ParlayANN, which support incremental updates, complete this operation an order of magnitude faster than CAGRA and GANNS. The difference arises because CAGRA and GANNS lack incremental

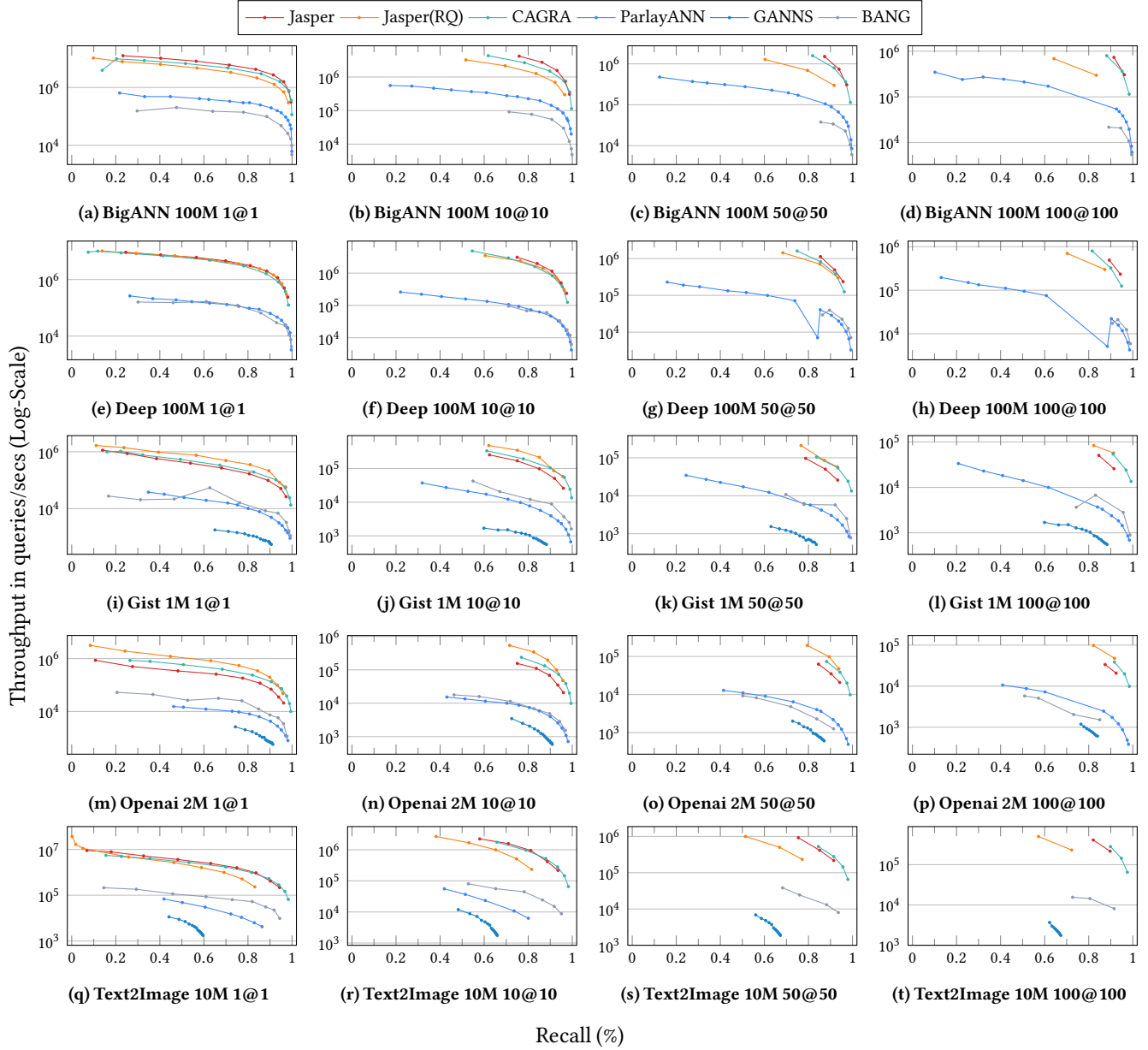


Figure 8: Query recall/throughput curves for various ANNS indexes across five datasets on Nvidia A100 GPU. We report recall at 1@1, 10@10, 50@50, and 100@100. Y-axis is on log-scale. X-axis is recall.

update support: each batch of new vectors requires rebuilding the entire index from scratch.

Takeaways. *Batch-parallel construction offers best-in-class performance for construction while still allowing for incremental updates. Insertion performance does not decrease linearly with increasing index size, leading to strong scaling as the dataset size increases.*

6.3 Queries

Here we evaluate the approximate nearest neighbor search (ANNS) performance of Jasper against other ANNS indexes.

Low-dimensional vector datasets: BigANN and Deep. For the low-dimensional vector datasets, Jasper is the fastest index for all recall values supported, with peak throughput of 13.2 million queries/sec at .31 recall. On BigANN, it is followed by Jasper RaBitQ which has the second highest throughput. Jasper is the fastest ANNS index up to .9943 recall as it does not achieve an accuracy higher than that on BigANN. For Deep, CAGRA is the second fastest index for all recall values tested. CAGRA achieves a higher maximum accuracy on these datasets, with peak accuracy of .9999 for BigANN 1@1 and .983 for Deep 1@1.

Jasper is the fastest for the low-dimensional vector datasets due to its optimized vector loads. For small beam sizes, latency hiding is not as effective as there is relatively little work performed per vector. This means that reducing latency of loads improves the performance of these kernels, as GPU compute spends less time waiting..

Takeaways. *By removing every shared memory component possible, Jasper can run more queries per SM. This, along with the optimized vector loads for latency reduction, allow for best-in-class query performance on small vector datasets for all beam widths supported.*

High-dimensional vector datasets: Gist and OpenAI. On the high-dimensional vector datasets Gist and OpenAI, distance calculations dominate the run time. To measure the cost of operations, we add cycle counters to every operation in the search kernel. When running Jasper exact on both BigANN and Gist, we see a 17.8× increase in the cycles taken for distance calculations in Gist, with distance calculations becoming the most expensive operation in the entire search.

The large vector size of these datasets benefits quantization as it can reduce the compute and memory requirements of distance calculations. On these datasets, Jasper RaBitQ is the fastest algorithm for all sizes it supports, with peak throughput over 3 million queries/sec and recall up to .94 for 50@50. After Jasper RaBitQ, CAGRA has the second best throughput-recall trade-off curve for all $k@k$ recall curves, followed by Jasper, then ParlayANN and GANNS.

All indices suffer significant performance reductions on these datasets due to the high volume of data transfers and distance calculations. On these datasets, the use of quantization results in an 8× decrease in memory transfer due to reduced vector size. The results in Figure 12 confirm our hypothesis that direct vector comparison is necessary for efficient quantized performance on GPUs: all versions of CAGRA PQ benchmarked against do not show improvements in performance, while Jasper RaBitQ is up to 60% faster than the exact implementation.

Takeaways. *On high-dimensional vectors, the 8× memory reduction of quantized vector loads leads to higher arithmetic intensity and faster throughput. However, this speedup is only practically achievable when the quantized vectors are directly comparable: PQ vectors achieve the same memory reduction but fail to provide speedups.*

Text2Image. Text2Image uses maximal inner product (MIPS) MIPS for distance instead of Euclidean. This makes construction and querying this dataset difficult as MIPS does not preserve the triangle inequality. Having a triangle inequality is necessary for the space to be metric and is crucial in constructing good search graphs using the Vamana indexing method. Without this property, graph construction can have poor results as there is no correlation between the neighbors of a given vector: it is possible to be "close" to a target query vertex and "far" from all of its neighbors, making pruning impossible. To overcome this, ANNS indices convert MIPS into a Euclidean space by adding one extra dimension. This allows for graph construction but comes at the cost of one extra dimension.

Both the Jasper and Jasper RaBitQ implementations suffer from reduced performance on this dataset, as the conversion from MIPS to Euclidean distance reduces the accuracy compared to systems like CAGRA that can construct the graph using the original MIPS distance calculation. Jasper has the highest recall/throughput trade-off on this dataset until .9 recall, at which point CAGRA shows the highest recall/throughput trade-off. Due to the low dimensions (200), Jasper

	Beam width=1			Beam width=256		
	BigANN	Deep	Gist	BigANN	Deep	Gist
Tiled	8,398,510	6,701,980	690,150	94,949	88,599	23,994
Chunked	9,610,650	7,621,580	768,947	94,904	88,555	24,161

Table 5: Difference in tiled and chunked load strategies. The numbers are throughput of queries in millions of queries per second. For smaller beam widths, the chunked strategy provides lower latency as all load requests are issued simultaneously. For higher beam widths, total throughput dominates, resulting in identical performance.

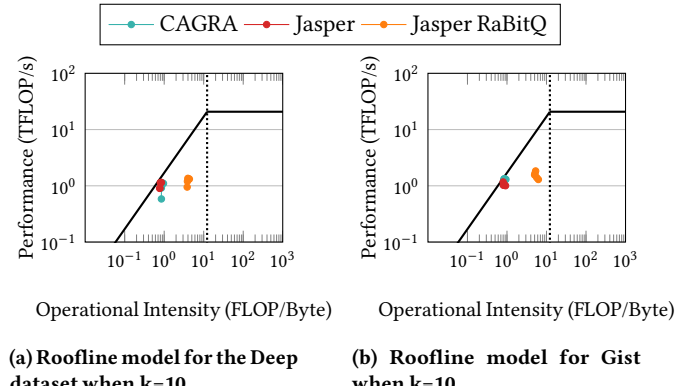


Figure 9: Roofline analysis of the Deep and Gist search kernels for Jasper, Jasper RaBitQ, and CAGRA. Y-axis is on log-scale.

exact shows higher performance than Jasper RaBitQ, with Jasper RaBitQ showing reduced recall due to the MIPS distance calculation.

Takeaways. *As MIPS does not form a metric space, the Vamana algorithm struggles to produce a good search graph due to the triangle inequality being necessary for RobustPrune. Jasper has the highest throughput for most beam widths supported, but struggles to reach high recall compared to CAGRA, as NN-descent does not require a metric space to form the graph.*

6.4 RaBitQ quantization

Jasper RaBitQ reduces the volume of data loaded during queries, which improves performance on datasets with high-dimensional vectors. As shown in Figure 8, the exact-distance version of Jasper is slower than CAGRA on Gist and OpenAI, but Jasper RaBitQ closes this gap and surpasses CAGRA at the same recalls despite using a lossy representation. For example, on OpenAI at 90% recall (10@10), Jasper RaBitQ is 3× faster than Jasper. On Deep, which has smaller vectors, Jasper RaBitQ performs comparably to the exact version.

On datasets with low-dimensional vectors, such as BigANN and Text2Image, Jasper RaBitQ is slightly slower than exact distance computation due to its lossy representation and additional arithmetic overhead. However, Jasper RaBitQ remains valuable in memory-constrained settings because it reduces device memory usage, allowing more vectors to reside on the GPU. We compare Jasper RaBitQ against other quantization methods in Section 6.6.

6.5 Roofline analysis

We use roofline analysis [43] to characterize Jasper’s performance on both low-dimensional (Deep) and high-dimensional (Gist) vectors. Figure 9 compares the arithmetic intensity and achieved throughput of Jasper and Jasper RaBitQ against CAGRA with $K = 10$.

Across both datasets, the roofline results indicate that Jasper operates predominantly in a memory-bound regime, with operational intensities are clustered tightly around 0.7–0.95 FLOP/byte. On DEEP, Jasper achieves peak throughputs around 0.89–1.14 TFLOP/s at these low intensities, closely tracking the sloped bandwidth roof. This behavior is consistent with ANNS workloads dominated by irregular memory accesses during graph traversal, where additional compute cannot be fully exploited without increasing data reuse. The comparable intensity–performance envelope between Jasper and CAGRA on Deep suggests that both systems are similarly constrained by memory bandwidth, with performance differences largely attributable to constant-factor effects such as traversal efficiency and kernel scheduling rather than fundamental compute utilization.

In contrast, Jasper RaBitQ significantly increases operational intensity, where intensities rise to 5.0–6.2 FLOP/byte and achieved performance reaches up to 1.83 TFLOP/s. This rightward shift on the roofline indicates substantially improved arithmetic reuse, allowing Jasper RaBitQ to move closer to the compute roof and escape the strict bandwidth-bound regime observed in Jasper. Overall, these results show that Jasper RaBitQ’s reordering and query-time computation strategies improve performance by reducing memory traffic.

Takeaways. *Jasper and CAGRA are both memory bound and have similar roofline plots close to the roofline, suggesting that the kernels are achieving close to ideal performance. Quantization significantly increases the arithmetic intensity of the kernels, suggesting that quantized ANNS performance can still be improved significantly.*

6.6 Microbenchmarks

We now present four microbenchmarks analyzing key design decisions in Jasper. First, we evaluate how tile-based loading affects throughput. Second, we examine the impact of partitioning warps into smaller worker units. Third, we measure how block size affects performance across different vector dimensions. Finally, we compare our RaBitQ implementation against PQ on the GPU.

Load microbenchmark. The load microbenchmark measures performance of our coalesced load implementation against a traditional tiled approach. In this microbenchmark we run both approaches and query BigANN, Deep, and Gist with beam widths 1 and 256, the smallest and largest beam widths supported. The results for this benchmark are in Table 5. For small beam widths, we see that the performance of the coalesced loads is consistently higher than tiled loads. This is due to the reduced latency from issuing load instructions simultaneously. For low beam widths, using coalesced loads provides a 14% performance increase as loads are sent and thus return faster, reducing the latency of the query. For larger beam widths, latency hiding means that total memory bandwidth dominates performance, and the coalesced loads show no measurable change in performance.

Tile microbenchmark. We compare our coalesced load implementation against traditional tiled loading on BigANN, Deep, and Gist using beam widths of 1 and 256 (Table 5). At small beam widths, coalesced loads provide a 14% throughput improvement by issuing

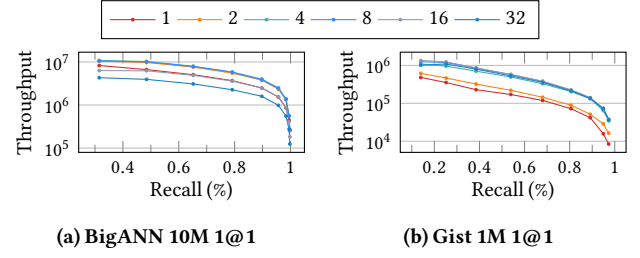


Figure 10: Varying Tile size for BigANN and Gist. Throughput is in millions of queries per second.

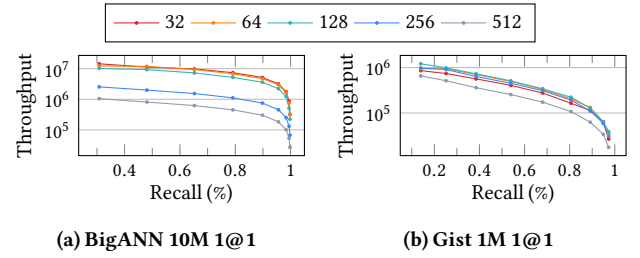


Figure 11: Varying Block size for BigANN and Gist. Throughput is in millions of queries per second.

all load instructions simultaneously, reducing latency. At large beam widths, sufficient in-flight operations hide memory latency, so both approaches achieve similar throughput.

Block microbenchmark. Block size controls the trade-off between parallelism within a query and the number of concurrent queries per SM. Larger blocks assign more threads to each query; smaller blocks allow more queries to execute simultaneously, increasing memory-level parallelism. Results are shown in Figure 11a and Figure 11b.

For datasets with high-dimensional vectors (Gist, OpenAI), reducing block size improves performance until reaching 128 threads per block. Below this point, performance drops because distance computation becomes the bottleneck—there are too few threads to efficiently process each high-dimensional vector. For datasets with low-dimensional vectors (BigANN, Deep), distance computation is not the bottleneck. Smaller block sizes consistently improve performance by enabling greater memory parallelism. The optimal configuration uses 32 threads per block (a single warp per query), allowing 32 concurrent queries per SM and maximizing memory throughput.

Quantization microbenchmark. We compare quantization methods in Figure 12, measuring query throughput for Jasper (exact and RaBitQ) against CAGRA (exact and PQ). To ensure a fair comparison, we evaluate CAGRA’s PQ under two configurations: one matching Jasper RaBitQ’s compression ratio (4× reduction), and one using CAGRA’s default heuristics.

CAGRA’s exact distance computation is highly optimized for high-dimensional vectors and slightly outperforms Jasper’s exact computation. However, Jasper RaBitQ outperforms all CAGRA variants, including exact. CAGRA’s PQ achieves throughput similar to its exact version despite reducing memory footprint, the scattered lookups required for PQ distance computation negate any bandwidth

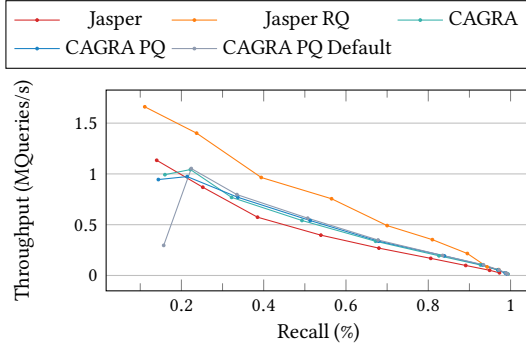


Figure 12: Different quantization method’s query performance for Gist 1M 1@1

savings. These results confirm that RaBitQ is more effective than product quantization for GPU workloads.

7 Related work

In this section, we discuss the current state of the art in ANNS indexes that are not directly evaluated against Jasper. These are indexes that are either 1) superseded in performance by the current state-of-the-art, 2) do not have a publicly available implementation, or 3) are complementary to ANNS but not directly comparable.

FAISS. FAISS [9] is a library for efficient similarity search and clustering of vectors. It provides a broad collection of approximate and exact nearest neighbor algorithms, with efficient CPU and GPU implementations. FAISS supports multiple indexing strategies and techniques, including inverted file indexes, product quantization, three-level quantization, HNSW, anisotropic vector quantization, NSG, and binary multi-index hashing. On GPUs, FAISS leverages massive parallelism to accelerate both index construction and query processing, making it a common choice for large-scale similarity search workloads.

SONG. SONG [46] is a GPU ANNS that uses a fixed-rank ANN search graph for ANN queries. SONG uses bulk computation processing, a priority queue, and a cuckoo-filter to efficiently process queries. To improve performance, the algorithm only considers vertices with a distance smaller than those in the current Top-K. This reduces the number of vertices that need to be remembered, but comes at the cost of additional compute to re-measure distances. They additionally optimize hash table/filter usage by deleting keys that fall out of the current top-K, as these nodes can’t be re-added to the search due to having too far of a distance from the query.

GTS. GTS [47] is a GPU tree-based ANN index for exact K-nearest neighbors. This tree is constructed using a bulk-synchronous algorithm. Along with the main tree structure, the node value for each vector is written into a table. Objects are mapped to nodes using a FFT pivot selection, and the list is partitioned to place the objects contiguously next to each other in device memory. This process repeats to further partition nodes until all leaves in the tree are sufficiently small. A bulk *cache list* is used to record streaming updates until a sufficient number of updates are recorded. The entire tree structure is then recomputed. For queries, they utilize a batched algorithm

based on iterative range queries: A list of the top- K closest nodes is kept, and all children in a level are considered unless their distance from the query falls outside of the top- K largest distance - this search is iteratively refined until the leaves are reached and a final set of top- K results can be extracted. During updates, new keys are held in a buffer that is checked during every query. If the buffer becomes too large, then entire tree is regenerated.

NEOS. NEOS [15] is an ANNS tool library that pins GPU memory in CPU user space and offers several optimizations to improve GPU buffer design such as pinning NVME memory, custom CPU to GPU memory copies, and faster CPU-GPU polling. NEOS is not a vector index but instead is a buffer tool that can be used by other indices such as HNSW. NEOS uses a large unsorted buffer to aggregate incoming requests; using the parallelism of an A100 and cuBLAS matrix operations, the entirety of the buffer can be checked with low latency. This allows for other vector managers to process streaming updates while only possessing a batch insertion API, which can make these applications more flexible without compromising throughput.

FusionANNs. FusionANNs [38] is a coprocessor vector index that uses the GPU as a helper for performing expensive distance comparisons. The index is based off of the posting lists used in SPANN - the authors find that the main limit to scalability in the original SPANN algorithm is the distance comparisons used when selecting the top- K from posting lists. Therefore, the product-quantized representation of the vectors is kept on GPU memory. Posting lists are generated by using hierarchical balanced clustering [14]. During a query, the CPU traverses the graph to find the closest posting lists to the target query. The IDs from these posting lists are sent to the GPU, and the distances for every item in the lists is calculated in parallel. This listing is returned to the CPU, where a heuristic re-ranking algorithm is executed to locate the best vectors. The full vectors are then loaded from SSD, and an exact distance comparison is executed to determine the final set. The code for FusionANNs is not publicly available.

LoRANN. LoRANN [17] introduces a new clustering methods called reduced-rank regression (RRR). This method is a built-in replacement for product quantization, and can be used both in setting clusters and for querying the posting lists of a cluster from the IVF. In RRR, the data is processed as a full batch, with the goal of minimizing the value of $\beta_{RRR} = \arg\min_{\beta} \|Y - X\beta\|_F^2$, where Y are the true nearest neighbors. A fast randomized algorithm is used to compute the nearest neighbors of the training set, and predictions are made via a matrix multiplication $\hat{y} = x^T \beta_{RRR}$. To perform operations efficiently, the training set is first cast into a low-dimensional space by taking the eigenvectors from PCA. The result of this is then quantized via 8-bit integer quantization. These operations can be efficiently processed on both CPU and GPU. In testing, the authors find that their implementation can replace PQ in FAISS to improve performance on high-dimensional vector datasets.

8 Conclusion

In this work, we demonstrate that porting approximate nearest neighbor search (ANNS) to GPUs can yield substantial performance improvements, enabling high-throughput query processing and effective colocation with downstream machine learning workloads. However, the extreme degree of parallelism exposed by modern GPUs introduces new challenges: GPU ANNS algorithms often fail

to achieve maximum performance due to synchronization overheads and limited shared memory. Our results show that carefully simplifying ANNS kernels to reduce shared memory usage can significantly increase throughput and achieve higher parallelism.

We further observe that the state-of-the-art GPU ANNS kernels such as CAGRA already operate close to the architectural roofline, indicating that raw compute optimizations offer diminishing returns. At beam width=256, Jasper achieves 50% higher FLOP/S than CAGRA, but this value is 69% of the peak possible throughput throughput for this arithmetic intensity - suggesting only a further 1.44x speedup is possible in this kernel.

Consequently, future performance gains must come primarily from reducing memory traffic. Quantization techniques that are directly comparable to full-precision baselines, such as RaBitQ, provide a promising path forward by preserving accuracy while reducing memory transfer by up to 8 \times . This reduction not only improves performance on large-scale vector datasets but also increases arithmetic intensity, suggesting that substantial headroom remains for further gains through quantization-aware ANNS designs.

9 Acknowledgments

This work was supported by the NSF grant 2517201 and 2513656. Additionally, we would like to thank Harsha Vardhan Simhadri and Magdalene Dobson Manohar for insightful discussions early in the project.

References

[1] Jade Alglave, Mark Batty, Alastair F. Donaldson, Ganesh Gopalakrishnan, Jeroen Ketema, Daniel Poetzl, Tyler Sorensen, and John Wickerson. 2015. GPU Concurrency: Weak Behaviours and Programming Assumptions. In *Proceedings of the Twentieth International Conference on Architectural Support for Programming Languages and Operating Systems* (Istanbul, Turkey) (ASPLOS '15). Association for Computing Machinery, New York, NY, USA, 577–591. doi:10.1145/2694344.2694391

[2] Ilias Azizi, Karima Echihabi, and Themis Palpanas. 2025. Graph-Based Vector Search: An Experimental Evaluation of the State-of-the-Art. *Proceedings of the ACM on Management of Data* 3, 1 (Feb. 2025), 1–31. doi:10.1145/3709693

[3] Artem Babenko and Victor Lempitsky. 2015. The Inverted Multi-Index. *IEEE Transactions on Pattern Analysis and Machine Intelligence* 37, 6 (June 2015), 1247–1260. doi:10.1109/tpami.2014.2361319

[4] Imane Belahyane, Mouad Mammass, Hasna Abiou, and Ali Idarrou. 2020. *Graph-Based Image Retrieval: State of the Art*. Springer International Publishing, 299–307. doi:10.1007/978-3-030-51935-3_32

[5] Jon Louis Bentley. 1975. Multidimensional binary search trees used for associative searching. *Commun. ACM* 18, 9 (Sept. 1975), 509–517. doi:10.1145/361002.361007

[6] Guy E. Blelloch, Daniel Anderson, and Laxman Dhulipala. 2020. ParlayLib - A Toolkit for Parallel Algorithms on Shared-Memory Multicore Machines. In *Proceedings of the 32nd ACM Symposium on Parallelism in Algorithms and Architectures (SPAA '20)*. ACM, 507–509. doi:10.1145/3350755.3400254

[7] Mayur Datar, Nicole Immorlica, Piotr Indyk, and Vahab S. Mirrokni. 2004. Locality-sensitive hashing scheme based on p-stable distributions. In *Proceedings of the twentieth annual symposium on Computational geometry (SoCG04)*. ACM, 253–262. doi:10.1145/997817.997857

[8] Wei Dong, Charikar Moses, and Kai Li. 2011. Efficient k-nearest neighbor graph construction for generic similarity measures. In *Proceedings of the 20th international conference on World wide web (WWW '11)*. ACM. doi:10.1145/1963405.1963487

[9] Matthijs Douze, Alexandre Guizha, Chengqi Deng, Jeff Johnson, Gergely Szilvassy, Pierre-Emmanuel Mazaré, Maria Lomeli, Lucas Hosseini, and Hervé Jégou. 2024. The Faiss library. doi:10.48550/ARXIV.2401.08281

[10] R. A. Finkel and J. L. Bentley. 1974. Quad trees—a data structure for retrieval on composite keys. *Acta Informatica* 4, 1 (1974), 1–9. doi:10.1007/bf00288933

[11] Jianyang Gao and Cheng Long. 2024. RaBitQ: Quantizing High-Dimensional Vectors with a Theoretical Error Bound for Approximate Nearest Neighbor Search. *Proceedings of the ACM on Management of Data* 2, 3 (May 2024), 1–27. doi:10.1145/3654970

[12] Siddharth Gollapudi, Neel Karia, Varun Sivashankar, Ravishankar Krishnaswamy, Nikit Begwani, Swapnil Raz, Yiyong Lin, Yin Zhang, Neelam Mahapatro, Premkumar Srinivasan, Amit Singh, and Harsha Vardhan Simhadri. 2023. Filtered-DiskANN: Graph Algorithms for Approximate Nearest Neighbor Search with Filters. In *Proceedings of the ACM Web Conference 2023 (WWW '23)*. ACM, 3406–3416. doi:10.1145/3543507.3583552

[13] Xiaoyi Gu, Leman Akoglu, and Alessandro Rinaldo. 2019. Statistical Analysis of Nearest Neighbor Methods for Anomaly Detection. In *Advances in Neural Information Processing Systems*, H. Wallach, H. Larochelle, A. Beygelzimer, F. d'Alché-Buc, E. Fox, and R. Garnett (Eds.), Vol. 32. Curran Associates, Inc. https://proceedings.neurips.cc/paper_files/paper/2019/file/805163a0f0f128e473726ccda5f91bac-Paper.pdf

[14] J. A. Hartigan and M. A. Wong. 1979. Algorithm AS 136: A K-Means Clustering Algorithm. *Applied Statistics* 28, 1 (1979), 100. doi:10.2307/2346830

[15] Yuchen Huang, Xiaopeng Fan, Song Yan, and Chuliang Weng. 2024. Neos: A NVMe-GPUs Direct Vector Service Buffer in User Space. In *2024 IEEE 40th International Conference on Data Engineering (ICDE)*. IEEE, 3767–3781. doi:10.1109/icde60146.2024.00289

[16] Piotr Indyk and Rajeev Motwani. 1998. Approximate nearest neighbors: towards removing the curse of dimensionality. In *Proceedings of the thirtieth annual ACM symposium on Theory of computing - STOC '98 (STOC '98)*. ACM Press, 604–613. doi:10.1145/276698.276786

[17] Elias Jääsäri, Ville Hyvönen, and Teemu Roos. 2024. LoRANN: Low-Rank Matrix Factorization for Approximate Nearest Neighbor Search. In *Advances in Neural Information Processing Systems*, A. Globerson, L. Mackey, D. Belgrave, A. Fan, U. Paquet, J. Tomczak, and C. Zhang (Eds.), Vol. 37. Curran Associates, Inc., 102121–102153. https://proceedings.neurips.cc/paper_files/paper/2024/file/b939da3932e88ded5e9b08026e35069d-Paper-Conference.pdf

[18] Suhas Jayaram Subramanya, Fnu Devvrit, Harsha Vardhan Simhadri, Ravishankar Krishnawamy, and Rohan Kadekodi. 2019. DiskANN: Fast Accurate Billion-point Nearest Neighbor Search on a Single Node. In *Advances in Neural Information Processing Systems*, H. Wallach, H. Larochelle, A. Beygelzimer, F. d'Alché-Buc, E. Fox, and R. Garnett (Eds.), Vol. 32. Curran Associates, Inc. https://proceedings.neurips.cc/paper_files/paper/2019/file/09853c7fb1d3f8ee67a61b6bf4a7f8e6-Paper.pdf

[19] William B. Johnson and Joram Lindenstrauss. 1984. Extensions of Lipschitz mappings into a Hilbert space. 189–206 pages. doi:10.1090/comm/026/737400

[20] H Jégou, M Douze, and C Schmid. 2011. Product Quantization for Nearest Neighbor Search. *IEEE Transactions on Pattern Analysis and Machine Intelligence* 33, 1 (Jan. 2011), 117–128. doi:10.1109/tpami.2010.57

[21] Yury Malkov, Alexander Ponomarenko, Andrey Logvinov, and Vladimir Krylov. 2014. Approximate nearest neighbor algorithm based on navigable small world graphs. *Information Systems* 45 (Sept. 2014), 61–68. doi:10.1016/j.is.2013.10.006

[22] Yu A. Malkov and D. A. Yashunin. 2020. Efficient and Robust Approximate Nearest Neighbor Search Using Hierarchical Navigable Small World Graphs. *IEEE Transactions on Pattern Analysis and Machine Intelligence* 42, 4 (April 2020), 824–836. doi:10.1109/tpami.2018.2889473

[23] Magdalena Dobson Manohar, Zheqi Shen, Guy Blelloch, Laxman Dhulipala, Yan Gu, Harsha Vardhan Simhadri, and Yihan Sun. 2024. ParlayANN: Scalable and Deterministic Parallel Graph-Based Approximate Nearest Neighbor Search Algorithms. In *Proceedings of the 29th ACM SIGPLAN Annual Symposium on Principles and Practice of Parallel Programming (PPoPP '24)*. ACM, 270–285. doi:10.1145/3627535.3638475

[24] Marvin Minsky and Seymour A. Papert. 2017. *Perceptrons: An Introduction to Computational Geometry*. The MIT Press. doi:10.7551/mitpress/11301.001.0001

[25] Rajeev Motwani, Assaf Naor, and Rina Panigrahy. 2008. Lower Bounds on Locality-Sensitive Hashing. *SIAM Journal on Discrete Mathematics* 21, 4 (Jan. 2008), 930–935. doi:10.1137/050646858

[26] NVIDIA. [n. d.]. Nvidia A100 tensor core GPU | Data sheet | 1. <https://www.nvidia.com/content/dam/en-zz/Solutions/Data-Center/a100/pdf/nvidia-a100-datasheet-nvidia-us-2188504-web.pdf>

[27] Camilla Birch Okkels, Martin Aumüller, and Arthur Zimek. 2024. *On the Design of Scalable Outlier Detection Methods Using Approximate Nearest Neighbor Graphs*. Springer Nature Switzerland, 170–184. doi:10.1007/978-3-031-75823-2_14

[28] Hiroyuki Ootomo, Akira Naruse, Corey Nolet, Ray Wang, Tamas Feher, and Yong Wang. 2024. CAGRA: Highly Parallel Graph Construction and Approximate Nearest Neighbor Search for GPUs. arXiv:2308.15136 [cs.DS] <https://arxiv.org/abs/2308.15136>

[29] Derrick Quinn, Mohammad Nouri, Neel Patel, John Salihu, Alireza Salemi, Sukhan Lee, Hamed Zamani, and Mohammad Alian. 2025. Accelerating Retrieval-Augmented Generation. In *Proceedings of the 30th ACM International Conference on Architectural Support for Programming Languages and Operating Systems, Volume 1* (Rotterdam, Netherlands) (ASPLOS '25). Association for Computing Machinery, New York, NY, USA, 15–32. doi:Quinn2025

[30] Md. Shaikh Rahman, Syed Maudud E. Rabbi, and Muhammad Mahbubur Rashid. 2024. Optimizing Domain-Specific Image Retrieval: A Benchmark of FAISS and Annoy with Fine-Tuned Features. ArXiv abs/2412.01555 (2024). <https://api.semanticscholar.org/CorpusID:274437371>

[31] Deepjyoti Roy and Mala Dutta. 2022. A systematic review and research perspective on recommender systems. *Journal of Big Data* 9, 1 (May 2022). doi:10.1186/s40537-022-00592-5

[32] Erich Schubert, Arthur Zimek, and Hans-Peter Kriegel. 2015. *Fast and Scalable Outlier Detection with Approximate Nearest Neighbor Ensembles*. Springer International Publishing, 19–36. doi:10.1007/978-3-319-18123-2_2

[33] Harsha Vardhan Simhadri, George Williams, Martin Aumüller, Matthijs Douze, Artem Babenko, Dmitry Baranichuk, Qi Chen, Lucas Hosseini, Ravishankar Krishnawamy, Gopal Srinivasa, Suhas Jayaram Subramanya, and Jingdong Wang. 2022. Results of the NeurIPS'21 Challenge on Billion-Scale Approximate Nearest Neighbor Search. ArXiv 2205.03763 [cs.LG] <https://arxiv.org/abs/2205.03763>

[34] Aditi Singh, Suhas Jayaram Subramanya, Ravishankar Krishnawamy, and Harsha Vardhan Simhadri. 2021. FreshDiskANN: A Fast and Accurate Graph-Based ANN Index for Streaming Similarity Search. doi:10.48550/ARXIV.2105.09613

[35] Pradeep Kumar Singh, Pijush Kanti Dutta Pramanik, Avick Kumar Dey, and Prasenjit Choudhury. 2021. Recommender systems: an overview, research trends, and future directions. *International Journal of Business and Systems Research* 15, 1 (2021), 14. doi:10.1504/ijbsr.2021.111753

[36] Sivic and Zisserman. 2003. Video Google: a text retrieval approach to object matching in videos. In *Proceedings Ninth IEEE International Conference on Computer Vision*. IEEE, 1470–1477 vol.2. doi:10.1109/iccv.2003.1238663

[37] Yiping Sun, Yang Shi, and Jiaolong Du. 2024. A Real-Time Adaptive Multi-Stream GPU System For Online Approximate Nearest Neighborhood Search. In *Proceedings of the 33rd ACM International Conference on Information and Knowledge Management (CIKM '24)*. ACM, 4906–4913. doi:10.1145/3627673.3680054

[38] Bing Tian, Haikun Liu, Yuhang Tang, Shihai Xiao, Zhiuhui Duan, Xiaofei Liao, Hai Jin, Xuecang Zhang, Junhua Zhu, and Yu Zhang. 2025. Towards High-throughput and Low-latency Billion-scale Vector Search via CPU/GPU Collaborative Filtering and Re-ranking. In *23rd USENIX Conference on File and Storage Technologies (FAST 25)*. USENIX Association, Santa Clara, CA, 171–185. <https://www.usenix.org/conference/fast25/presentation/tian-bing>

[39] Karthik Venkatasubba, Saim Khan, Somesh Singh, Harsha Vardhan Simhadri, and Jyothi Vedurada. 2025. BANG: Billion-Scale Approximate Nearest Neighbour Search Using a Single GPU. *IEEE Transactions on Big Data* 11, 6 (Dec. 2025), 3142–3157. doi:10.1109/tbdata.2025.3581085

[40] Hui Wang, Wan-Lei Zhao, Xiangxiang Zeng, and Jianye Yang. 2021. Fast k-NN Graph Construction by GPU based NN-Descent. In *Proceedings of the 30th ACM International Conference on Information & Knowledge Management (CIKM '21)*. ACM, 1929–1938. doi:10.1145/3459637.3482344

[41] Shijie Wang, Wenqi Fan, Yue Feng, Lin Shanru, Xinyu Ma, Shuaiqiang Wang, and Dawei Yin. 2025. Knowledge Graph Retrieval-Augmented Generation for

LLM-based Recommendation. In *Proceedings of the 63rd Annual Meeting of the Association for Computational Linguistics (Volume 1: Long Papers)*. Association for Computational Linguistics, 27152–27168. doi:10.18653/v1/2025.acl-long.1317

[42] Tevin Wang, Jingyuan He, and Chenyan Xiong. 2024. RAGViz: Diagnose and Visualize Retrieval-Augmented Generation. In *Proceedings of the 2024 Conference on Empirical Methods in Natural Language Processing: System Demonstrations*. Association for Computational Linguistics, 320–327. doi:10.18653/v1/2024.emnlp-demo.33

[43] Samuel Williams, Andrew Waterman, and David Patterson. 2009. Roofline: an insightful visual performance model for multicore architectures. *Commun. ACM* 52, 4 (April 2009), 65–76. doi:10.1145/1498765.1498785

[44] Yan Xia, Kaiming He, Fang Wen, and Jian Sun. 2013. Joint Inverted Indexing. In *2013 IEEE International Conference on Computer Vision*. IEEE, 3416–3423.

doi:10.1109/iccv.2013.424

[45] Yuanhang Yu, Dong Wen, Ying Zhang, Lu Qin, Wenjie Zhang, and Xuemin Lin. 2022. GPU-accelerated Proximity Graph Approximate Nearest Neighbor Search and Construction. In *2022 IEEE 38th International Conference on Data Engineering (ICDE)*. IEEE, 552–564. doi:10.1109/icde53745.2022.00046

[46] Weijie Zhao, Shulong Tan, and Ping Li. 2020. SONG: Approximate Nearest Neighbor Search on GPU. In *2020 IEEE 36th International Conference on Data Engineering (ICDE)*. IEEE. doi:10.1109/icde48307.2020.00094

[47] Yifan Zhu, Ruiyao Ma, Baihua Zheng, Xiangyu Ke, Lu Chen, and Yunjun Gao. 2024. GTS: GPU-based Tree Index for Fast Similarity Search. *Proceedings of the ACM on Management of Data* 2, 3 (May 2024), 1–27. doi:10.1145/3654945